Mitoparan and target-selective chimeric analogues: Membrane translocation and intracellular redistribution induces mitochondrial apoptosis

Sarah Jones [a,*], Cecile Martel [b], Anne-Sophie Belzacq-Casagrande [b],
Catherine Brenner [b], John Howl [a]

[a] Research Institute in Healthcare Science, University of Wolverhampton, Wulfruna Street, Wolverhampton, WV1 1SB UK
[b] University of Versailles/St Quentin, CNRS UMR 8159, Bat Buffon, 45 avenue des Etats-Unis, 78035 Versailles, France

Abstract

Mastoparan, and structurally-related amphipathic peptides, may induce cell death by augmentation of necrotic and/or apoptotic pathways. To more precisely delineate cytotoxic mechanisms, we determined that $[Lys^{5,8}Aib^{10}]$mastoparan (mitoparan) specifically induces apoptosis of U373MG and ECV304 cells, as demonstrated by endonuclease and caspase-3 activation and phosphatidylserine translocation. Live cell imaging confirmed that, following translocation of the plasma membrane, mitoparan specifically co-localizes with mitochondria. Complementary studies indicated that mitoparan induces swelling and permeabilization of isolated mitochondria, through cooperation with a protein of the permeability transition pore complex VDAC, leading to the release of the apoptogenic factor, cytochrome c. N-terminal acylation of mitoparan facilitated the synthesis of chimeric peptides that incorporated target-specific address motifs including an integrin-specific RGD sequence and a Fas ligand mimetic. Significantly, these sychnologically-organised peptides demonstrated further enhanced cytotoxic potencies. We conclude that the cell penetrant, mitochondriotoxic and apoptogenic properties of mitoparan, and its chimeric analogues, offer new insights to the study and therapeutic induction of apoptosis.
© 2008 Elsevier B.V. All rights reserved.

Keywords: Cell penetrating peptides; Apoptosis; Mitochondria; Chimerism; Mastoparan

1. Introduction

The mechanism(s) by which the tetradecapeptide mastoparan (MP, H-INLKALAALAKKIL-NH₂) and structural analogues mediate cell death remains unresolved. Biophysical evidence indicates that in aqueous solution the structure of MP is largely disordered, but upon interaction with biological membranes and lipidic environments MP adopts an amphipathic α-helical conformation [1,2]. This ability of MP and its analogues to interact and insert into biological membranes has prompted a non-specific necrotic model of MP-induced cell death [3]. Accordingly, MP facilitates random pore formation in the plasma membrane leading to the increased permeability of extracellular cations and subsequent cell lysis [4]. Conversely, in cell free systems MP binds specific intracellular targets integral to signal transduction pathways that orchestrate apoptosis. Cell free models of neuronal apoptosis using isolated mitochondria have shown that MP, through interaction with mitochondrial membranes [5] and opening of mitochondrial permeability transition pores [6,7], promotes the release of apoptogenic proteins such as cytochrome c [8], which consequentially leads to activation of the caspase cascade [8]. The cytotoxic actions of MP have also been attributed to MP sharing homology with the amphipathic helix forming death domains of the tumour necrosis factor receptor-1 (TNFR-1) and Fas [9].

MP is more widely acknowledged as a receptor-independent, allosteric regulator of heterotrimeric G proteins, predominantly G_i and G_o. More specifically, MP presents a cationic hydrophilic

face on the inner side of the plasma membrane that mimics the G protein binding domain of G protein-coupled receptors [1,2, 10,11]. However, the cytotoxic action of MP is probably independent of *pertussis toxin* (PTX)-sensitive G proteins (G_i/G_o) [12] and there is growing evidence to suggest that the diverse biological properties of MP are not restricted to those events regulated by heterotrimeric G proteins [13]. This phenomenon is particularly relevant to its chimeric analogues [13] and especially the relatively inert cell penetrant MP chimera transportan 10 that is widely employed as an effective peptide vector [14].

The ex vitro characteristics of MP, as a facilitator of mitochondrial permeability transition, has lead to proposals that MP could be of utility in cancer therapeutics [15], provided that MP is encapsulated in a tumour-selective delivery system. Features of such a construct would necessitate cell penetration in addition to specific tumour homing properties. We have recently reported that our highly efficacious MP analogue [Lys^{5,8}Aib^{10}] MP (mitoparan; mitP) promotes a concentration-dependent decrease in U373MG astrocytic tumour cell viability [16]. Thus, one major aim of the present study was to confirm that mitP penetrates the plasma membrane of both U373MG astrocytoma and ECV304 bladder carcinoma cells, and to identify intracellular loci of action that subsequently induce apoptotic events in these cancer cell lines.

A rapidly expanding field of peptide and cell penetrating peptide research has been dedicated to the selective targeting of tumours by engineering constructs that incorporate cell-specific or tissue-specific address motifs [17,18]. Peptidyl address motifs could enhance the selectivity of drug delivery leading to a probable reduction in non-selective side effects, whilst the improved cellular uptake offered by cell penetrating peptides (CPP), undoubtedly enhances bioavailability. The utility of mitP, as a novel cell penetrant mitochondriotoxic peptide, was thus further studied by analysis of the cytotoxic profiles of chimeric peptides that incoporated peptidyl address motifs as N-terminal extensions. These investigations included an RGD motif which confers an ability to selectively bind cell adhesion receptors (integrins) [19]. Phage display technologies have also identified RGD as a glioma-specific ligand [20], whilst integrin $\alpha_V\beta_3$ expressed on ECV304 cells binds extracellular matrix components in an RGD-dependent manner [21]. Additionally, these studies also included the more recently described Fas ligand mimetic sequence WEWT, since this tetrameric sequence could bind Fas to activate the extrinsic apoptotic pathway [22,23].

Our adopted chimeric strategy may also be referred to as a sychnologic organisation, a term originally adopted by Schwyzer [24] to describe the organisation of recognition elements of peptide hormones. The main diagnostic feature of sychnologic peptides is the spatial separation of address and message motifs that are themselves continuous in nature. However, it is not uncommon that N-terminal extension or covalent attachment with an address motif may severely impact upon the bioactivity of the message. Thus, a second objective of this study was to establish that the desirable pharmacodynamic parameters of mitP can be incorporated as a component of chimeric target-selective peptides without abrogation of cytotoxic efficacy.

2. Materials and methods

2.1. Materials

N-α-*tert*-Butyloxycarbonyl-Cys(3-Nitro-2-pyridinesulfanyl)-OH (Boc-Cys(Npys)-OH), Mas17 and cyclo(-RGD*f*V) were purchased from Bachem (St. Helens, UK). All other materials for solid phase peptide synthesis were from Novabiochem (Beeston, UK). Cell culture medium was obtained from PAA Laboratories Ltd (Linz, Austria). All other chemical reagents were purchased from Sigma Aldrich (Dorset, UK) unless otherwise stated.

2.2. Peptide synthesis, purification and analysis

With the exception of Mas17 and cyclo(-RGD*f*V), peptides were manually synthesized (0.1 mmol scale) on Rink amide methylbenzhydrylamine (MBHA) resin employing an *N*-α-Fmoc protection strategy with 2-(1-H-Benzotriazole-1-yl)-1,1,3,3-tetramethyluronium hexafluorophosphate/*N*-Hydroxybenzotriazole) (HBTU/HOBt) activation. Crude peptides were purified to apparent homogeneity by semi-preparative scale HPLC [25]. Fluorescent peptides, to be used in confocal live cell imaging, were synthesized by N-terminal acylation with 6-carboxy-tetramethylrhodamine or 5-carboxy-fluorescein (Novabiochem, Beeston, UK). The predicted masses of all peptides used (average M+ H$^+$) were confirmed to an accuracy of +1 by matrix-assisted laser desorption ionization (MALDI) time of flight mass spectrometry (Kratos Kompact Probe operated in positive ion mode).

2.3. Cell culture

U373MG cells were maintained in DMEM and ECV304 cells in M199 in a humidified atmosphere of 5% CO_2 at 37 °C. Both media contained L-glutamine (0.1 mg/ml) and were supplemented with 10% (wt/vol) fetal bovine serum (FBS), penicillin (100 U/ml) and streptomycin (100 μg/ml).

2.4. MTT assays of cellular viability

Cell viability was measured by the 3-(4,5-dimethylthazol-2-yl)-2,5-diphenyl tetrazolium bromide (MTT) conversion assay [26]. U373MG and ECV304 cells were cultured as above in 96 well plates and washed in medium without serum prior to assay. Cells were treated with MP, mitP and chimeric analogues at 37 °C for the times indicated and further incubated with MTT (0.5 mg/ml) for 3 h at 37 °C. The insoluble formazan product was solubilized with DMSO. MTT conversion was determined by colorimetric analysis at 540 nm. Cell viability was expressed as a percentage of those cells treated with vehicle (medium) alone. Graphical representations of changes in cell viability and LD$_{50}$ values were calculated using GraphPad Prism 5 software and the sigmoidal dose–response function. Statistical analyses were performed using the non-parametric Mann–Whitney *U* test; set parameters were one-tailed from unpaired observations with confidence intervals set at 95% (GraphPad Prism 5).

Table 1
The predicted masses of all peptides were confirmed to an accuracy of ±1 by matrix-assisted laser desorption ionization (MALDI) time of flight mass spectrometry (Kratos Kompact *Probe* operated in positive ion mode)

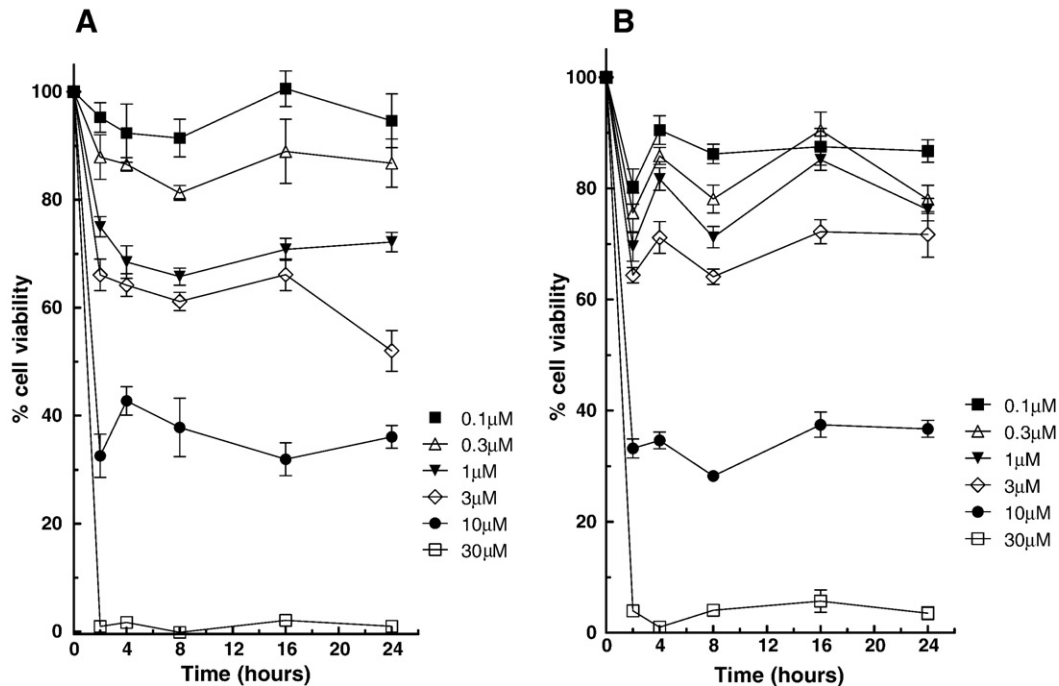| Peptide	Primary sequence	Predicted mW	Confirmed mW
MP	*H*-INLKALAALAKKIL-*NH$_2$*	1478.9	1479.0
mitP	*H*-INLKKLAKL(Aib)KKIL-*NH$_2$*	1617.1	1617.9
Z-Gly-RGD*f*-mitP	Z-GRGD*f*INLKKLAKL(Aib)KKIL-*NH$_2$*	2273.8	2274.0
Z-Gly-RGE*f*-mitP	Z-GRGE*f*INLKKLAKL(Aib)KKIL-*NH$_2$*	2287.9	2288.1
WEWT(Ahx) mitP	*H*-WEWT(Ahx)INLKKLAKL(Aib)KKIL-*NH$_2$*	2322.8	2322.3

Fig. 1. Temporal analyses of mitP-induced cytotoxicity. U373MG (A) and ECV304 cells (B) were exposed to varying concentrations of mitP (0.1–30 μM) for the time periods indicated. Cell viability was used to determine cytotoxicity and measured by MTT conversion. Cell viability was expressed as a percentage of those cells treated with vehicle (medium) alone. Data points are mean±S.E.M. from 3 experiments performed in triplicate.

2.5. Detection of DNA fragmentation in situ by TUNEL assay

Nuclear DNA fragmentation, a characteristic of apoptosis, was detected by the Tdt (terminal deoxynucleotidyl transferase)-mediated dUTP nick end labeling (TUNEL) assay according to manufacturers instructions (In Situ Cell Death Detection kit, TMR red, Roche, UK). U373MG and ECV304 cells were grown to sub confluence on cover slips in 6 well plates, washed and treated with peptides or vehicle alone (medium) for 2 h in medium without serum. Cells were washed with phosphate-buffered saline (PBS), pH 7.4 and fixed with 4% (wt/vol) formaldehyde in PBS for 1 h at room temperature. Fixed cells were permeabilized with 0.1% (vol/vol) Triton X-100 in 0.1% (wt/vol) sodium citrate at 4 °C for 2 min, then incubated for 1 h at 37 °C in a humidified atmosphere in the dark with TUNEL reaction mixture containing Tdt and TMR red-dUTP to label free 3′OH ends in the DNA. Cover slips were washed in PBS, air-dried and mounted on slides with Vectashield™ (Vector Laboratories Inc, Peterborough, UK) containing 4′6′ Diamidino-8-phenylindole dihydrochloride (DAPI) to counter stain double-stranded DNA in the nuclei. Samples were analyzed using a Carl Zeiss LSM 510 Meta confocal microscope. Positive controls were achieved by incubating fixed and permeabilized cells with DNase 1, grade 1 (3000 U/ml in 50 mM Tris–HCl, pH 7.5, 1 mg/ml BSA) for 10 min at room temperature to induced DNA strand breaks, prior to labeling procedure. Negative controls were achieved by incubating fixed and permeabilized cells in TUNEL reaction mixture without Tdt.

2.6. Confocal Microscopy, fluorescence detection and co-localization studies

Cells were plated out into 35 mm sterile glass base dishes (IWAKI, Japan) and grown to subconfluence in medium containing 10% (vol/vol) fetal bovine serum (FBS) and penicillin (100 U/ml) and streptomycin (100 μg/ml) and maintained in a humidified atmosphere of 5% CO_2 at 37 °C. Growing medium was gently removed and cells were washed once in pre-warmed stimulation medium (without phenol red, serum and penicillin streptomycin). Cells were incubated with fluorescent peptides diluted to a final concentration of 5 μM in stimulation medium, for the indicated time periods and at 37 °C in a humidified atmosphere of 5% CO_2. Cells were washed gently, 8 times in stimulation medium and incubated in 1 ml stimulation medium for the duration of the analysis. Cells were analyzed using a

Carl Zeiss LSM 510 Meta confocal microscope. For mitochondrial co-localization studies, cells were incubated with 200 nM Mitotracker® Green FM (Molecular Probes, Invitrogen, Paisley, UK) alongside fluorescent peptides. Quantitative co-localization was performed using the Carl Zeiss quantitative co-localization analysis software, incorporating an interactive scatter plot and data table linked to the images. Pixels showing an intensity above the background of both channels (background defined as, pixels in channel 1 only, e.g. rhodamine and pixels in channel 2 only, e.g. fluorescein) were designated as co-localized pixels. Data were collected from an average of 12 regions of interest, between 50–200 μm^2 and from 3 independent experiments. Co-localization (coloc) coefficients were calculated for the two different fluorophores according to the following equations: C1=pixels channel 1 coloc/pixels channel 1 total, C2=pixels channel 2 coloc/pixels channel 2 total and defined as relative number of co-localizing pixels in channel 1(designated rhodamine) or 2 (designated fluorescein), respectively, as compared to the total number of pixels above threshold. Overlap coefficients after Manders were also used to quantify co-localization. Coefficients generated values between 0 and 1. A

Table 2
LD_{50} values were calculated for all peptides using Graphpad Prism software

Peptide	LD_{50}	
	ECV304	U373MG
MP	30.26±0.05	26.49±0.04
MitP	6.81±0.05	7.92±0.12
Z-Gly-RGDf-mitP	1.40±0.13	4.79±0.16
Z-Gly-RGEf-mitP	4.71±0.05	7.45±0.03
Z-Gly-RGDf-mitP[1]	6.08±0.08	4.87±0.83
Z-Gly-RGDf-mitP+cyclo(-RGDfV)[1]	9.17±0.07	10.27±2.5
WEWT(Ahx)mitP	4.44±0.04	28.10±0.03

Data are expressed in μM as mean±S.E.M. from 3 separate experiments. Values were calculated following 24 h exposure to peptides. Exceptions are highlighted (1) where cell viability readings were measured following 2 h, a time point optimized for the addition of cyclo(-RGD-DPhe-Val) (300nM) without evidence of cellular detachment.

value of 0 indicated no co-localization, whereas a value of 1 indicated that all pixels were co-localized.

## 2.7. Measurement of caspase-8 activity

Caspase-8 activity was measured using the Caspase-8 Colorimetric Assay (R & D Systems, Abingdon, UK) according to manufacturers instructions. U373MG and ECV304 cells were cultured as above and distributed to 6 well plates to give 2×10^6 cells per well and exposed to peptides, diluted in stimulation media or vehicle (media alone), for the indicated time periods. Reactions were terminated by the addition of 100 µl ice-cold lysis buffer (R & D Systems, Abingdon, UK). Cell lysates were centrifuged for 1 min at 10,000 $\times g$ at 4 °C. Supernatants (50 µl) were transferred to a 96 well plate and incubated with 5 µl of caspase-8 co-lorimetric substrate conjugated to p-nitroanaline (IETD-pNA) and 50 µl reaction buffer (R & D Systems, Abingdon, UK) at 37 °C for 2 h. Absorbances were read on a microtitre plate reader at 405 nm and caspase-8 activity expressed as fold/basal. A recombinant caspase-8 enzyme (R & D Systems, Abingdon, UK) was used as a positive control.
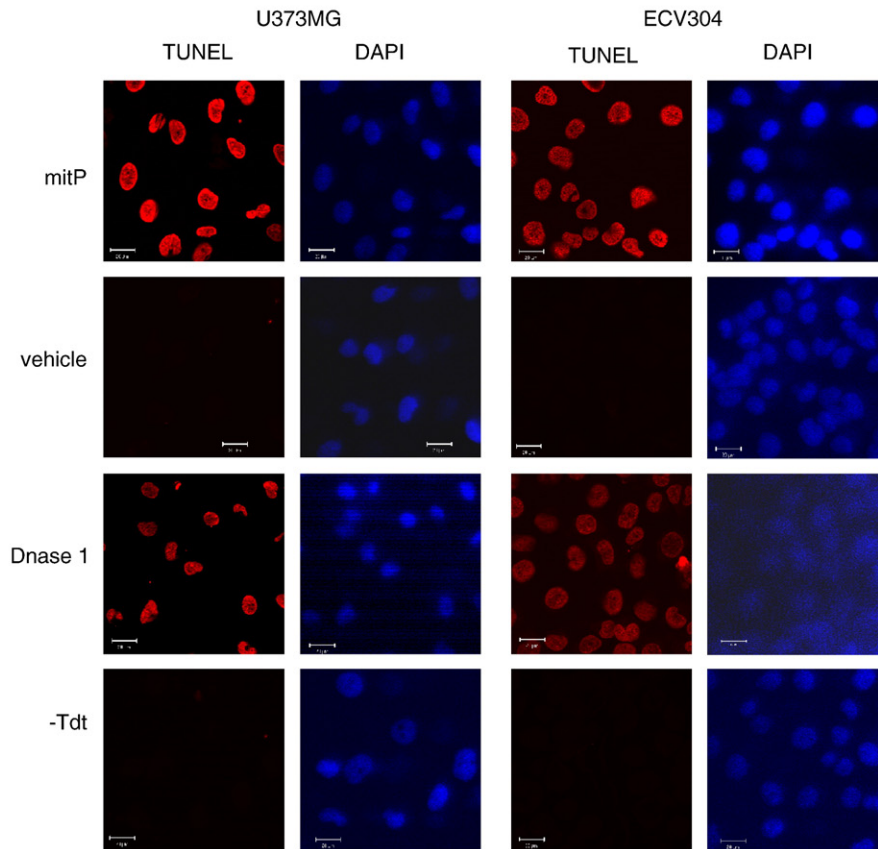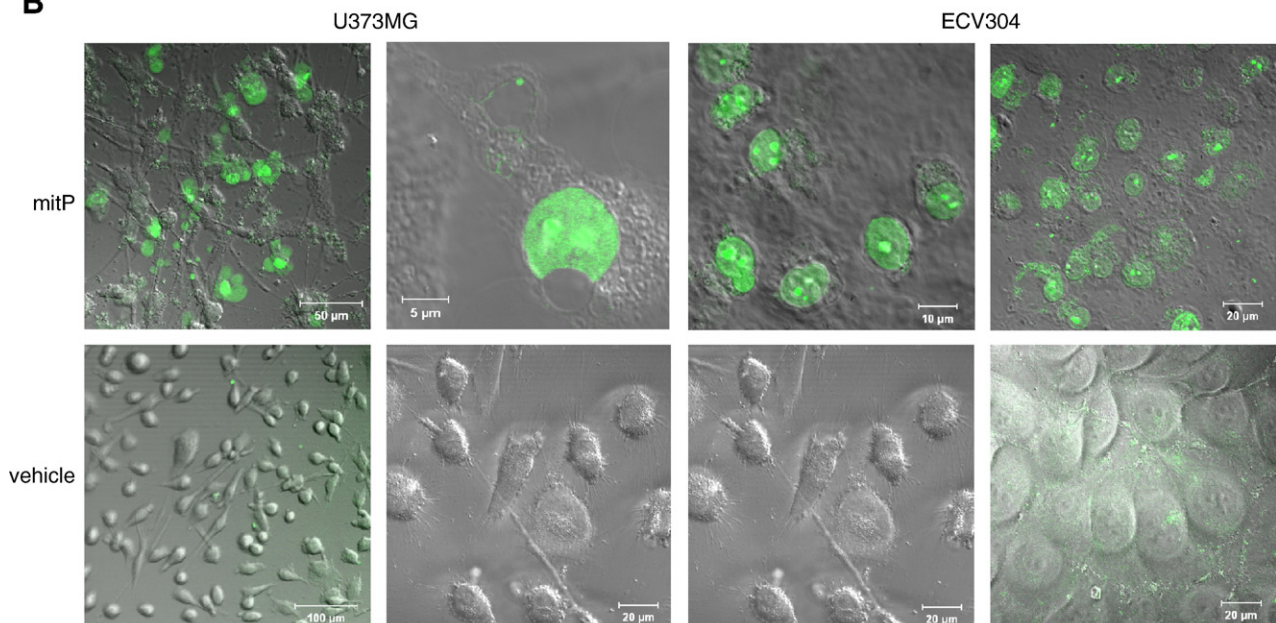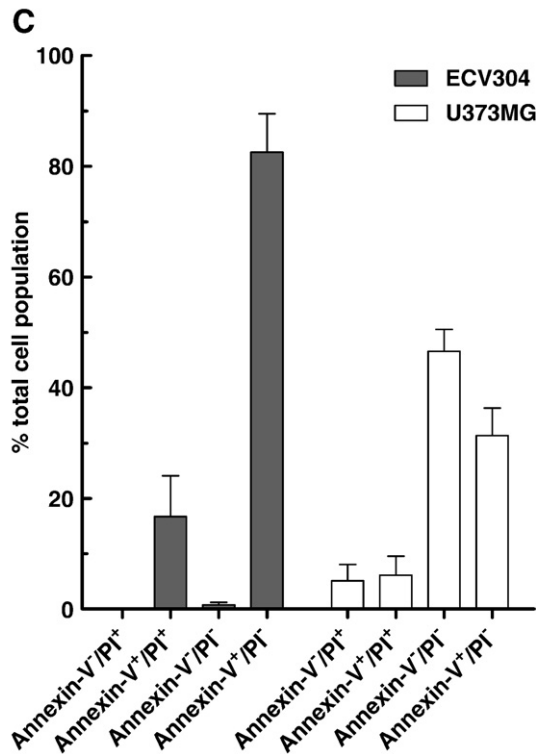
Fig. 2. MitP induces apoptosis as confirmed by DNA fragmentation and activation of caspase-3. (A) U373MG and ECV304 cells were treated with mitP (10 μM) or vehicle alone for 2 h. Cells were fixed in 4% (wt/vol) formaldehyde and permeabilized with 0.1% (vol/vol) Triton X-100. Nuclear DNA fragmentation, indicative of apoptosis, was detected by TUNEL in situ cell detection assay, TMR red (Roche) and cells were counterstained with DAPI to visualize nuclear DNA. Representative examples are shown. The appearance of TMR red fluorescence located in the nuclei of mitP-treated cells provides evidence of apoptosis, whereas DNA fragmentation is not evident in cells treated with vehicle alone (vehicle). Fixed and permeabilized cells were incubated with Dnase 1 (3000 U/ml) to induce DNA strand breaks, prior to the labeling procedure and therefore acts as a positive control (Dnase 1). DNA fragmentation is comparable to cells treated with mitP. As a negative control, fixed and permeabilized cells were treated with labeling solution without terminal deoxynucleotidyl transferase (−Tdt). Bars are 20 μm. (B) U373MG and ECV304 cells were treated with mitP (10 μM) or vehicle alone for 1 h. DEVD-NucView™ 488 Caspase-3 Substrate (Biotum, Inc) was added at a final concentration of 5 μM for a further 30 min and cells viewed by confocal live cell imaging. The cell permeable construct DEVD-NucView™ 488 Caspase-3 Substrate consists of a functional high affinity DNA-binding dye that is rendered inert by the highly negatively charged DEVD peptide substrate. Upon activation of caspase-3, the substrate is cleaved to release a functional DNA dye that subsequently migrates to the nucleus. Green fluorescence seen in the nuclei of mitP-treated cells indicates activation of caspase-3, compared to cells treated with medium alone (vehicle). (C) Flow cytometric analysis of annexin-V-fluorescein and propidium iodide (PI) staining of ECV304 and U373MG cells treated with mitP (10 μM). Quadrant statistics from 4 separate experiments were combined, represented graphically and demonstrate a predominant cell population of annexin-V$^+$/PI$^-$ (early apoptotic) compared to annexin-V$^+$/PI$^+$ (necrotic). Annexin-V$^-$/PI$^+$ represent dead cells and annexin-V$^-$/PI$^-$ represent viable cells.

2.8. Caspase-3

Detection of caspase-3 activity was measured using the DEVD-NucView™ 488 Caspase-3 Substrate (Biotium Inc, Cambridge Bioscience, Cambridge, UK) according to manufacturer's instructions. Cells were cultured as above and grown to 50% confluence in 35 mm sterile glass base dishes (IWAKI). Peptides were diluted in 1 ml of pre-warmed stimulation medium and incubated with cells to a final concentration of 10 μM for 1 h. DEVD-NucView™ 488 Caspase-3

substrate was added at a final concentration of 5 μM for a further 30 min. Nuclear staining and fluorescence was observed using a Carl Zeiss LSM 510 Meta confocal microscope.

2.9. Flow cytometry to determine annexin V and propidium iodide staining

Annexin V staining was measured using the Annexin-V-FLUOS staining kit (Roche, UK). 10^6 cells were treated with peptide, washed in Hanks balanced salt solution, trypsinized and centrifuged at 200 ×g for 5 min. The cell pellet was resuspended in 100 μl Annexin-V-FLUOS labelling solution containing annexin-V-fluorescein and propidium iodide and incubated for 15 min at 15–25 °C. Following the addition of 0.5 ml HEPES incubation buffer, fluorescence of annexin-V-fluorescein and propidium iodide was detected in FL-1 and FL-3 channels, respectively, on a BD FACS Calibar. Unstained and untreated cells were used to establish instrument settings and FL-1 and FL-3 cell populations were isolated to the first log decade. Stained and untreated cells were used to establish quadrant settings for dot plot analysis. Statistical analyses were performed using BD Cell Quest Pro software.

2.10. Isolation of mouse liver mitochondria

Mitochondria were isolated from mouse liver (Balb/c, female, 6–8 week old, Charles River, L'Arbresle, France) by differential centrifugations and purified on Percoll gradients [27]. Protein concentration was determined using the micro-BCA assay (Pierce Chemical Company, Rockford, Illinois).

2.11. Swelling, depolarization, inner membrane permeabilization and NADH ferricyanide assays

For swelling and depolarization measurements, mitochondria (25 μg protein) were diluted in an hypo-osmotic buffer (10 mM Tris–Mops, pH 7.4, 5 mM succinate, 200 mM sucrose, 1 mM Pi, 10 μM EGTA, 2 μM rotenone) containing various doses of Ca^{2+}, mitP, MP, Mas17 or vehicle alone. Mitochondrial swelling was immediately measured by the decrease in absorbance at 540 nm for 1000 s. Mitochondrial depolarization was measured by the rhodamine 123 fluorescence dequenching assay (1 μM, λexc: 485 nm, λem: 535 nm, Molecular Probes). Mitochondria (25 μg protein), were treated with or without inducers for 30 min at 37 °C to induce the swelling. Thereafter, DTNB (0.1 mM), acetylCoA (0.3 M) and oxaloacetate (0.5 mM) were added sequentially every 10 min and the absorbance at 412 nm was recorded for 2300 s. For NADH ferricyanide activity of VDAC, mitochondria (10 μg proteins) were equilibrated for 10 min at 37 °C in the presence of inducers or vehicle thereafter 250 μM NADH was added. After 15 min of incubation, addition of 300 μM ferricyanide was used to start the measurement of the fluorescence (λexc=360 nm; λem=465 nm). All assays were adapted from Tarze et al. [28] for 96-well plate analysis and were performed at 37 °C in a spectrofluorimeter (TECAN genios, TECAN, Grödig, Austria).

2.12. Cytochrome c release

Mitochondria (40 μg of protein), treated or not by CaCl$_2$, MitP and MP, were incubated for 30 min at 37 °C and then centrifuged at 6800 ×g for 10 min at 4 °C. Proteins contained in the supernatants were precipitated by methanol:chloroform [4:1 vol/vol], suspended in Laemmli sample buffer, separated by SDS-PAGE (15%) and transferred to PVDF membranes (Millipore, Hampshire, UK). After 2 h incubation at 20 °C with anti-cytochrome c (BD Biosciences, Le Pont de Clay, France), proteins were detected using the ECL method according to the manufacturer's instructions (Amersham Pharmacia Biotech, Rockford, IL).

3. Results

3.1. Peptide design

The ability of MP to form an amphipathic α−helix is a major determinant of its biological activity. Lysyl residues at positions 4,

11 and 12, together with the amino terminus, contribute to a cationic hydrophilic face [10]. Our initial design of mitP incorporated sequence permutations that were not only compatible with the formation of an amphipathic helix, but also enhanced the amphipathicity of MP by introducing additional lysyl residues (Lys[5], Lys[8]) within the hydrophilic face. This together with a known helix promoter, α-aminoisobutyric acid (Aib), produced a highly efficacious cytotoxic MP analogue [16]. In accordance with this observation, chimeric mitP analogues were rationally designed to maintain the amphipathicity of mitP. Z-Gly-RGD*f*-mitP conferred a cationic charge distribution that was compatible with an amphipathic α-helix. N-terminal blockade with Z-Gly and the inclusion of a D isomer of Phe(*f*), were additional modifications likely to improve the biostability of Z-Gly-RGD*f*-mitP. The control peptide Z-Gly-RGE*f*-mitP was also included in this study; since the conservative substitution of Glu for Asp in the core RGD sequence prevents integrin binding. N-terminal extension of mitP with the Fas ligand mimetic peptide WEWT was predicted to be incompatible with the formation of an extended amphipathic α-helix. Therefore, aminohexanoic acid was used as a flexible linker in the chimeric sequence of WEWT (Ahx)mitP.

To facilitate intracellular co-localization, mitP and related chimeric analogues were synthesized by N-terminal acylation with 6-carboxytetramethylrhodamine, to give the rhodamine-conjugated peptide Rho-mitP or, 5-carboxyfluorescein to give the fluorescein chimeric analogues Fluo-Gly-RGD*f*-mitP and Fluo-WEWT(Ahx)mitP.

Peptides were manually synthesized employing an N-α-Fmoc protection strategy and masses confirmed by matrix-assisted laser desorption ionization (MALDI) time of flight mass spectrometry (Table 1).

3.2. Mitoparan: cytotoxicity profiles and mechanisms of cell death

MitP promotes a concentration-dependent decrease in U373MG cell viability [16]. To extend the temporal characterisation of the cytotoxic actions of this peptide, changes in the viability of U373MG and ECV304 cells were analyzed over a 24 h time period with a peptide concentration range of 0.1–30 μM (Fig. 1). A maximal reduction in cell viability was achieved in 4 h with negligible alteration in cell viability thereafter. LD_{50} values (expressed as mean±S.E.M.) were taken at 24 h giving 7.92± 0.12 μM and 6.81+0.05 μM for U373MG and ECV304 respectively and demonstrate dramatically increased potencies compared to MP (LD_{50}=26.49±0.04 μM and 30.26±0.05 μM for U373MG and ECV304 respectively) under the same experimental conditions (Table 2).

Fig. 2A clearly indicates that inter-nucleosomal DNA fragmentation, as detected by in situ TUNEL staining, was evident in both U373MG and ECV304 cells following 2 h of treatment with mitP (10 μM). In addition, mitP (10 μM) promoted activation of caspase-3 (Fig. 2B) in both cell lines at 1.5 h. To firmly establish the mechanism of cell death, detection of phosphatidylserine translocation to the outer plasma membrane, a feature of early apoptosis, was measured by annexin-V staining and flow cyto-

metry. Since necrotic cells also expose phosphatidylserine owing to loss of membrane integrity, propidium iodide exclusion was carried out to discriminate between apoptosis and necrosis. Accordingly, following treatment with mitP (10 μM), data clearly show a predominant population of annexin-V positive and propidium iodide negative cells (early apoptotic) compared to the small percentage of cells that stained for both propidium iodide and annexin-V (necrotic) (Fig. 2C). Taken together, these data are consistent with apoptosis as the primary mechanism of mitP-induced cell death. On the basis of these findings, and given that MP binds mitochondrial membranes in cell free systems to promote release of cytochrome *c* [8], we speculated as to whether the observed apoptotic actions of mitP were attributable to its ability to translocate plasma membranes and to interact with mitochondria in living cellular systems. Confocal live cell imaging demonstrated that Rho-mitP (5 μM) assumed both an outer membrane and cytosolic distribution in U373MG cells after 30 min (Fig. 3A). Additional live cell images following 1 h of exposure to the peptide revealed a distinct co-localization with mitochondrial membranes in both U373MG and ECV304 cells (Fig. 3B). Moreover, this intracellular redistribution was accompanied by a loss of fluorescence associated with the plasma membrane. Quantitative co-localization was carried out giving colocalization coefficients for U373MG of 0.82±0.04 (channel 1; rhodamine) and 0.91±0.04 (channel 2; fluorescein) and for ECV304 of 0.85± 0.04 (channel 1; rhodamine) and 0.75±0.08 (channel 2; fluorescein). Overlap coefficients after Manders gave 0.78±0.02 and 0.74±0.01 for U373MG and ECV304, respectively. U373MG and ECV304 cells were also treated with rhodamine-conjugated MP (Rho-MP) under the same conditions. Confocal live cell imaging (Fig. 3C) and quantitative analysis for U373MG of 0.40±0.07 (channel 1; rhodamine) and 0.69±0.08 (channel 2; fluorescein) and for ECV304 of 0.26±0.04 (channel 1; rhodamine) and 0.21±0.06 (channel 2; fluorescein), demonstrated weak co-localization with mitochondria. Thus compared to MP, mitP demonstrates an increased propensity for mitochondrial localization.

3.3. Interactions of mitoparan with isolated liver mitochondria

Isolated mouse liver mitochondria were used to investigate direct actions of mitP on mitochondrial ultrastructure and function. Firstly, we observed that mitP induced an increase in mitochondrial volume, a loss of internal matrix material and rupture of the outer membrane (Fig. 4A). The effect of mitP was similar to the effects of Ca^{2+}, a prototypic permeability transition inducer and to that of MP. Secondly, 2 μM mitP simultaneously triggered mitochondrial swelling (Fig. 4B(i)), loss of transmembrane inner potential (ΔΨm) (Fig. 4B(ii)) and inner membrane permeabilization (Fig. 4B(iii)). The kinetics of swelling induced by mitP were similar to the kinetics elicited by MP, but differed drastically from that of Ca^{2+}. A dose-response study demonstrated that 2 μM was optimal to induce swelling of maximal amplitude (Fig. 4C(i)).

To gain additional insights into the molecular mechanisms of mitochondrial alteration induced by mitP in comparison to MP, we used several pharmacological agents known to
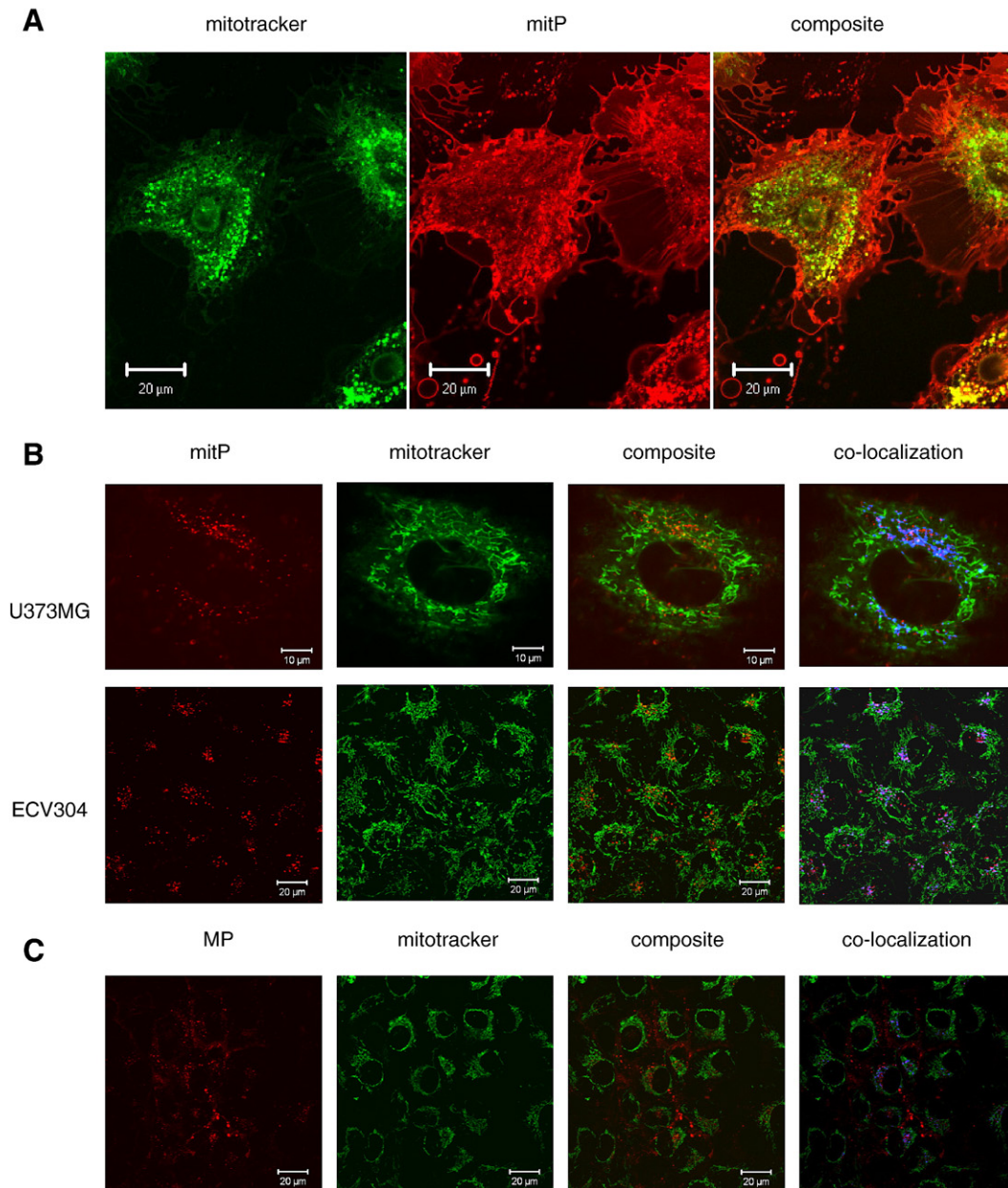
Fig. 3. MitP penetrates plasma membranes to co-localize with mitochondria. Cells were treated with 5 µM Rho-mitP and 200 nM Mitotracker® Green FM (Molecular Probes, Invitrogen) and viewed by confocal live cell imaging using a Carl Zeiss LSM 510 Meta. (A) At 30 min, Rho-mitP assumed both an outer membrane and cytosolic distribution, a representative image is shown here for U373MG cells. (B) Live cell images of U373MG and ECV304 captured following 1 h peptide exposure. Rho-mitP now assumes a predominant mitochondrial distribution. (C) MP demonstrates a decreased propensity for mitochondrial localization. Cells were treated for 1 h with 5 µM Rho-MP and 200 nM Mitotracker®. Live cell images of ECV304 cells are shown here as a representative sample. Pixels having an intensity above the single-labelled pixels for fluorescein (Mitotracker®) and rhodamine are indicative of co-localization. Co-localizing pixels are shown here in blue. An average of 12 regions of interest were selected using the Carl Zeiss quantitative co-localization analysis software and co-localization coefficients were calculated from 3 separate experiments. Representative examples are shown.

modulate mitochondrial inner membrane permeability. Of these, only the VDAC-targeting agents glutamate (GLU) [29] and 4,4′-diisothiocyanatostilbene-2,2′-disulfonic acid (DIDS) [30], partially or totally inhibited mitP-induced mitochondrial swelling (Fig. 4C(ii)). In contrast, cyclosporin A, an inhibitor of the interaction between the adenine nucleotide translocator (ANT) and cyclophilin D [31]; ATP, a ligand of the ANT; and N-acetyl cystein (NAC) [32], an anti-oxidant, had no preventive effect on mitP and MP-induced swelling. In addition, mitP-induced swelling was unaffected by 5 mM ethylene glycol-bis

(beta-aminoethyl ether)-N,N,N′,N′-tetraacetic acid (EGTA), a calcium chelator. These results indicate that mitochondrial toxicity induced by mitP may be mediated by a specific interaction with VDAC (Fig. 4C(ii)). Significantly, the inhibition of mitP-induced swelling was of a magnitude larger than that of MP (+20%), suggesting an enhanced specificity of the VDAC-mitP interaction. To test this hypothesis, we measured the NADH ferricyanide activity of VDAC in the presence of mitP and found that mitP exerted an inhibitory effect giving an EC_{50} of 1.84 ± 0.22 µM (Fig. 4D).

Finally, we determined the capacity of mitP to promote the release of cytochrome c (Fig. 4E). When co-incubated for 30 min with isolated mitochondria, mitP induced a dose-dependent re-

lease of cytochrome c from the intermembrane space to the external medium. This effect was lower than that induced by Ca^{2+}, but similar to that induced by mastoparan and correlated with a
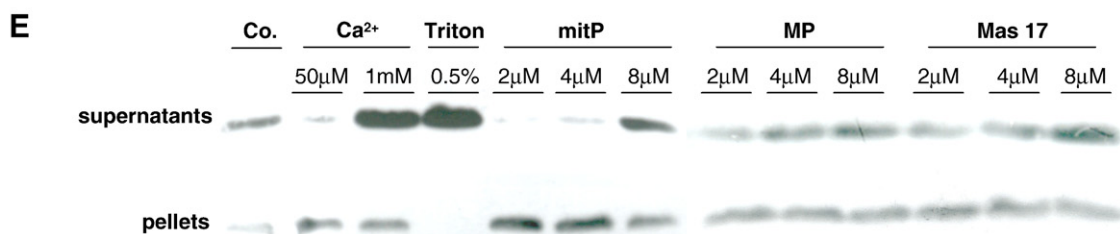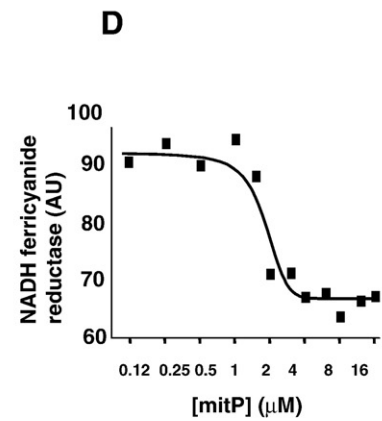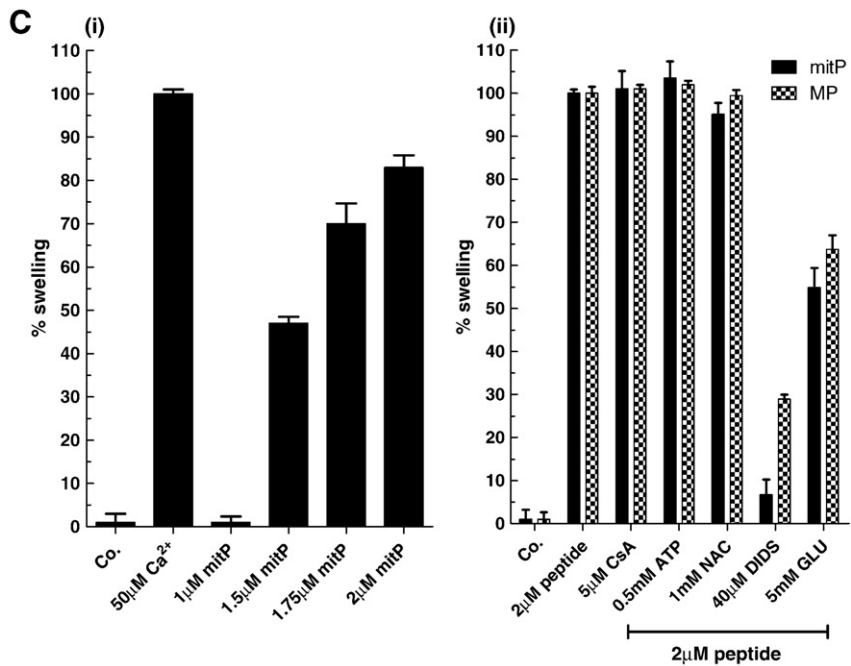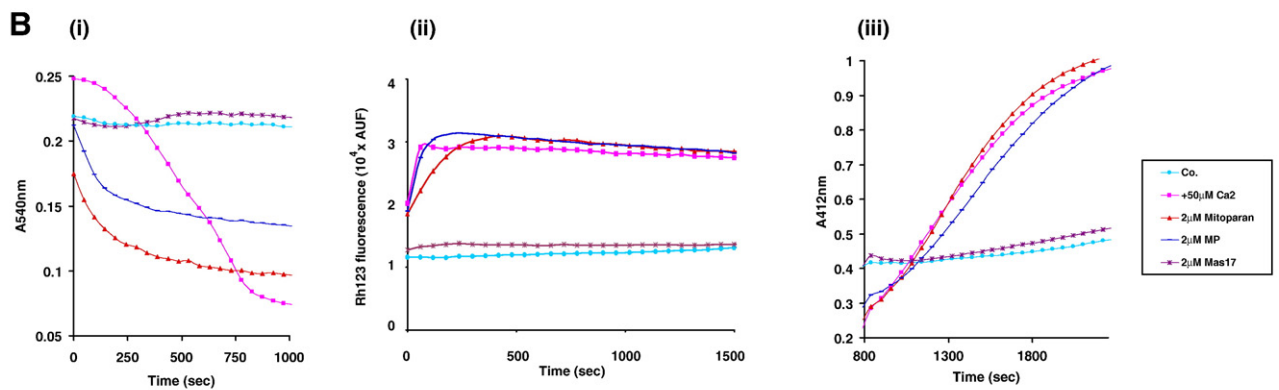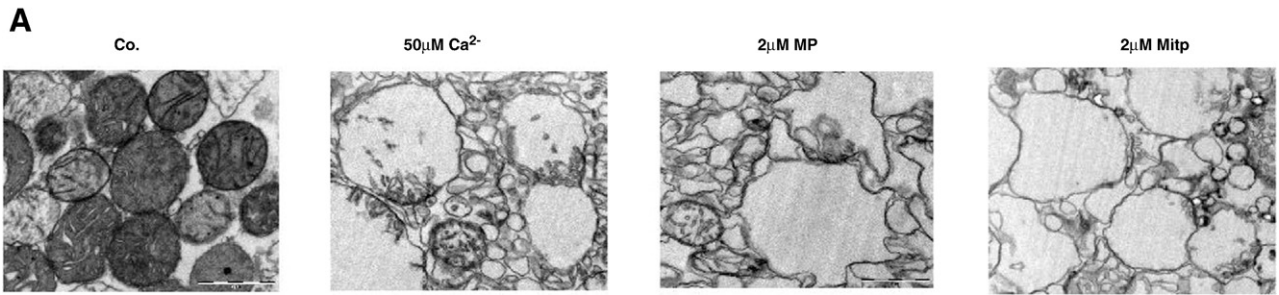
decreased content of cytochrome c within the mitochondria. This indicated that mitP induces a direct complete mitochondrial membrane permeabilization process, in line with its capacity to elicit mitochondrial apoptosis.

3.4. Apoptotic chimeric analogues of mitoparan: Z-Gly-RGDf-mitP

Dose-dependent cytotoxicity was maintained in ECV304 and U373MG cells following N-terminal extension of mitP with the integrin specific motif RGD. Moreover, in ECV304 cells, Z-Gly-RGDf-mitP demonstrated an enhanced potency (1.40±0.13 μM) compared to mitP alone (6.81±0.05 μM, $P=0.0286$) and the sequence variant Z-Gly-RGEf-mitP (4.71± 0.05 μM, $P=0.0286$) (Fig. 5A, Table 2). Similar results using the sequence variant Z-Gly-RGEf-mitP were obtained for U373MG cells (Table 2). To confirm the specificity of our RGD containing mitP analogue, ECV304 cells were pre-incubated with the integrin antagonist cyclic RGD peptide, cyclo(-RGDfV) [33]. Given that cyclo(-RGDfV) is a potent inhibitor of cell adhesion, cells viability readings were taken at 2 h and at a competing ligand concentraion of 300nM, conditions optimized to allow for viability readings without cellular detachment. Addition of cyclo (-RGDfV) reduced the potency of Z-Gly-RGDf-mitP from 6.08± 0.08 μM to 9.17±0.07 μM, $P=0.05$, (Fig. 5B, Table 2). Treatment of U373MG cells with our integrin-targeting mitP analogue demonstrated that Z-Gly-RGDf-mitP was moderately more potent ($LD_{50}=4.79±0.16$ μM) than mitP ($LD_{50}=7.92±0.12$ μM) on this cell line, $P=0.05$, (Fig. 5C, Table 2). Similarly, addition of cyclo(-RGDfV) to U373MG cells, under the above optimized conditions reduced the potency of Z-Gly-RGDf-mitP from 4.87± 0.83 μM to 10.27±2.5 μM (Table 2).

To confirm the mechanism of cell death both cell lines were treated with Z-Gly-RGDf-mitP (10 μM) for 2 h and assayed for DNA fragmentation by in situ TUNEL staining. Fig. 5D clearly provides evidence for apoptosis as the mechanism of cell death.

Confocal live cell imaging was used to determine the subcellular distribution of fluorescein-conjugated Z-Gly-RGDf-mitP. Fig. 5E demonstrates that 5 μM Fluo-Gly-RGDf-mitP translocated to the intracellular environment of both ECV304 and U373MG cells.

3.5. Apoptotic chimeric analogues of mitoparan: WEWT(Ahx) mitP

Both cell lines were treated with our mitP analogue which incorporated the Fas ligand mimetic WEWT and assayed for cytotoxicity. Fig. 6A and Table 2 show that WEWT(Ahx)mitP ($LD_{50}=4.44±0.04$ μM) was moderately more potent than mitP ($LD_{50}=6.81±0.05$ μM) in ECV304 cells, $P=0.05$. Reports indicate that U373MG cells are resistant to Fas ligand-induced apoptosis (extrinsic pathway) through an observed down regulation of caspase-8 [34] and a reduced cell surface expression of Fas [35]. Similarly, data from our laboratory indicates that following 24 h treatment with tumour necrosis factor-α (TNF-α; 400 ng/ml), U373MG cell viability is relatively unaltered at 90.0%, whereas, cell viability is reduced to 66.0% under the same conditions in ECV304 cells ($P=0.0001$). A dramatically enhanced potency for WEWT(Ahx)mitP in ECV304 cells ($LD_{50}=4.44±0.04$ μM) was observed compared to U373MG ($LD_{50}=28.10±0.03$ μM), $P=0.05$, (Fig. 6B, Table 2). Moreover, the potency of WEWT(Ahx)mitP in U373MG cells was severely reduced compared to the parent cytotoxin mitP, on the same cell line ($LD_{50}=7.92±0.12$ μM), $P=0.05$, (Table 2). As with the integrin targeting mitP analogue, apoptosis was confirmed as the mechanism of cell death for both cell lines (Fig. 6E) and cellular penetration was confirmed by confocal live cell imaging (Fig. 6F).

3.6. Mitoparan and its chimeric analogues induce cell death independently of the extrinsic apoptotic pathway

Reports that U373MG cells are resistant to Fas-mediated apoptosis may offer a simple explanation for the observed enhancement in potency of WEWT(Ahx)mitP in ECV304 cells compared to U373MG and also suggests that activation of the extrinsic apoptotic pathway may account in part, for the cytotoxic mechanisms employed by WEWT(Ahx)mitP in ECV304 cells. Moreover, TNF-α (40 ng/ml) induced a statistically significant increase in caspase-8 activity in ECV304 cells of 1.60 fold compared to 1.10 fold in U373MG cells ($P=0.0159$) (Fig. 6C). However, Fig. 6C also indicates that WEWT(Ahx) mitP (10 μM, 30 μM) did not activate caspase-8 in ECV304

Fig. 4. Interaction of mitP with isolated mitochondria. (A) Morphology of mouse liver mitochondria treated with mitP. Isolated mitochondria were treated with Ca^{2+}, mitP or MP for 30 min and their morphology was studied by transmission electronic microscopy (TEM) and compared with untreated control preperations (Co). MitP induced similar alterations to Ca^{2+} and MP, as was observed by swelling, membrane rupture and loss of internal material in comparison to untreated mitochondria (Co.). Magnitude: ×12 000. (B) Swelling, loss of transmembrane inner potential (ΔΨm) and permeabilization of the inner mitochondrial membrane in response to mitP. Isolated mitochondria were treated with Ca^{2+}, mitP, MP, the inactive MP analogue Mas17 or control and absorbance at 540 nm was recorded for 1000 s to measure the swelling of the mitochondrial matrix (i). (ii) Mitochondria were incubated under the same conditions but in the presence of a ΔΨm-sensitive probe, Rh123. Fluorescence was recorded for 1500 s. (iii) Permeabilization of the inner mitochondrial membrane. Isolated mitochondria were treated as in (i) and absorbance measured at 412 nm for 2300 s. Experiments were repeated three times in triplicate. (C) Concentration-dependent increase in mitochondrial swelling in response to mitP and pharmacological inhibition. Increasing concentrations of mitP were added and mitochondrial swelling was evaluated by the decrease in absorbance at 540 nm for 1000 s. The effect of 50 μM Ca^{2+} was normalized to 100% (i). Various concentrations of inhibitors, 5 μM CsA, 0.5 mM ATP, 5 mM NAC, 0.5 mM GLU and 25 μM DIDS, were added to mitochondria 2 min before mitP or MP and swelling was measured. The effects of 2 μM mitP and MP were normalized to 100% (ii). Experiments were repeated three times in triplicate. (D) Inhibition of VDAC by mitP. NADH ferricyanide reductase activity was used as an indicator of VDAC function. A concentration-dependent decrease in enzyme activity in response to mitP allowed for determination of an EC_{50} value for mitP. Data were analyzed using the sigmoidal dose-response function of GraphPad Prism software. (E) Release of cytochrome c from the intermembrane space. Mitchondria (25 μg of proteins) were treated for 30 min at 37 °C by indicated agents and centrifuged. Supernatants and pellets, corresponding the released fraction and the pelleted mitochondria, were analyzed by western-blotting for the presence of cytochrome c (Cyt c).

cells. Similarly, WEWT(Ahx)mitP failed to activate caspase-8 in U373MG cells. Both cell lines were resistant to activation of caspase-8 by mitP (Fig. 6C). On the basis that after 30 min, Rho-mitP assumed both an outer membrane and intracellular

distribution, activation of caspase-8 was measured after 30 min under the above conditions. To refine and extend the above findings, activation of caspase-8 was measured up to 4 h following the treatment of ECV304 cells with WEWT(Ahx)
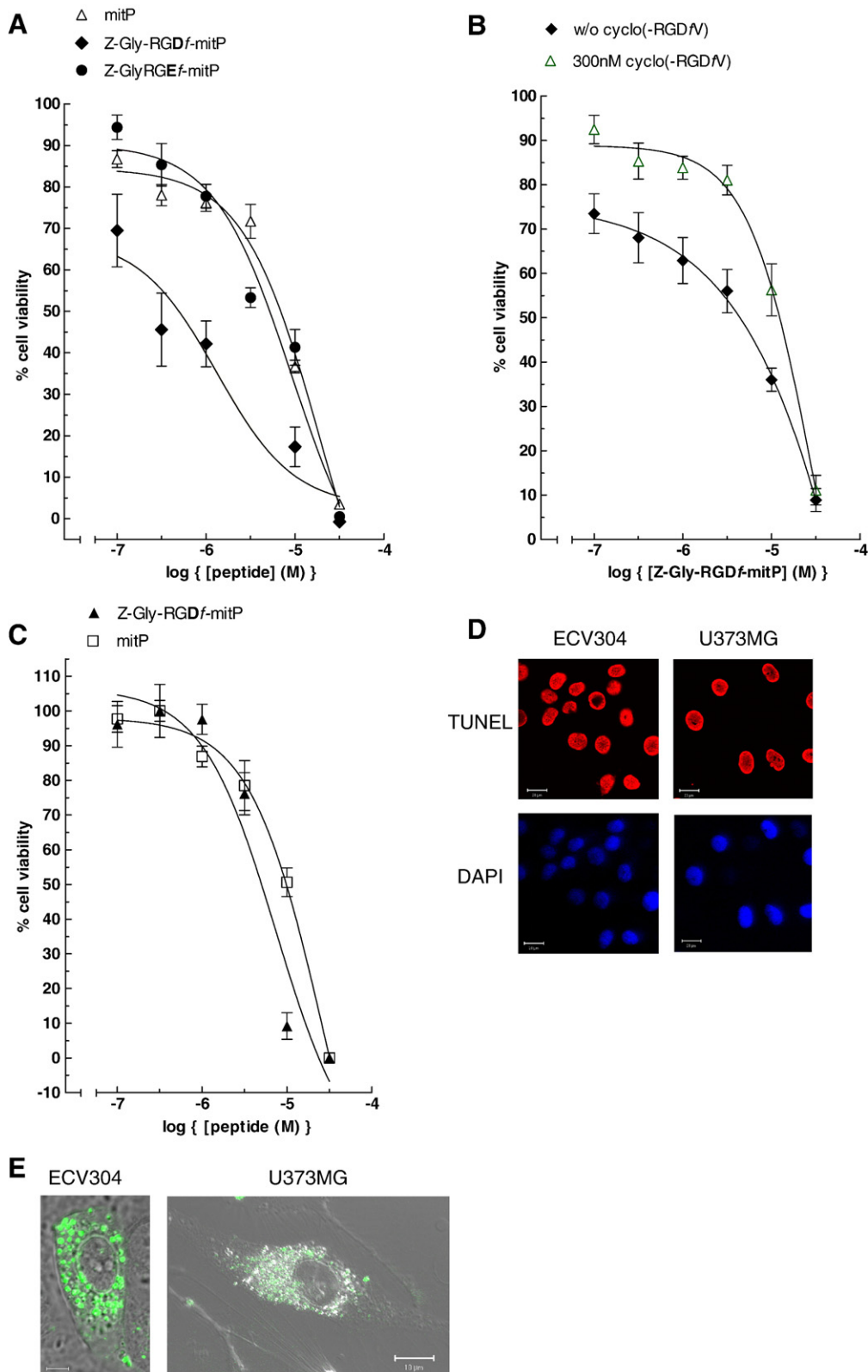
mitP and mitP. Neither peptide induced stimulation of caspase-8 in this cell line (Fig. 6D).

4. Discussion

Previously, MP has been considered as a non-specific inducer of plasma membrane pore formation. Data presented herein clearly shows that our novel MP analogue, mitP, exhibits both cell penetrant, mitochondriotoxic and apoptogenic properties, features that could be of potential therapeutic utility. Moreover, we have demonstrated that mitP can be modified to incorporate tissue-specific address motifs, constructs that not only maintain, but enhance the potency of mitP alone.

4.1. Mechanisms of mitoparan-mediated cell death

Fig. 3 clearly shows that at 30 min, Rho-mitP (5 μM) assumed an outer cell membrane and cytosolic distribution in living cells. After 1 h, Rho-mitP redistributed to co-localize with mitochondria, a feature that is not shared by its parent compound Rho-MP. A prerequisite to the execution of apoptosis is the caspase cascade, a series of cysteinyl aspartyl proteases that converge with the activation of caspase-3. Fig. 2 indicates that following 1.5 h, mitP (10 μM) induced activation of caspase-3 in both U373MG and ECV304 cells. Moreover, we have conclusively demonstrated that in cell free systems, mitP induces swelling, depolarization and permeabilization of the inner mitochondrial membrane. We suggest that, in living cellular systems, mitP induces apoptosis by targeting and interacting with mitochondrial membranes. Subsequently, enhanced membrane permeability augments the release of cytochrome c which consequentially leads to activation of the caspase cascade. Furthermore, given that both cell lines were resistant to the activation of caspase-8 by mitP and we observed apoptotic cell death in U373MG cells, a line that is apparently resistant to Fas-mediated apoptosis [34], it may be concluded that mitP does not induce apoptosis via the extrinsic pathway and death receptor mimicry as has been tentatively postulated previously for MP [9].

MitP has clearly demonstrated an enhanced cytotoxic potency (LD$_{50}$=7.92 μM and 6.81 μM for U373MG and ECV304, respectively) compared to MP (LD$_{50}$=26.49 μM and 30.26 μM for U373MG and ECV304, respectively) (Table 2), an observation that is more than likely reflected by its improved penetrative and mitochondrial localizing capacities in addition to its ability to alter mitochondrial membrane permeability

through an enhanced co-operation with a protein of the permeability transition pore complex (PTPC), VDAC. Indeed, previous reports that claim MP to be a potent facilitator of the permeability transition pore opening [6], show that at concentrations above 1 μM, MP-induced opening of permeability transition pores is insensitive to specific inhibition of PTP proteins and only at concentrations below 1 μM does MP facilitate pore opening which is susceptible to PTP protein inhibition. Though this study was largely restricted to observations using cyclosporin A, an inhibitor of the interaction between cyclophilin D and ANT, an observation that we also report, unlike MP, mitP clearly facilitates mitochondrial membrane permeability through specific interaction with VDAC even at concentrations above 1 μM.

As a point of conjecture, our data demonstrate an apoptotic response to acute chemical toxicity, a response that does not strictly concur with the true definition of programmed cell death, i.e. a tightly controlled selective elimination of cells that threaten organ homeostasis. But rather, by the very nature of its cell penetrant properties, mitP exploits intracellular apoptotic machinery to ultimately promote induction of the caspase cascade. Interestingly, following tissue injury or chemical insult, both features of apoptosis and necrosis are evident, an observation that has fuelled doubt as to apoptosis being the sole mechanism of cell death under these circumstances [36]. As a consequence, the author Lemasters proposes the introduction of a new definition of cell death for cells showing signs of apoptosis following acute chemical toxicity, termed necrapoptosis [36]. Such a definition promotes a less rigid and probably more accurate description of cell death to chemical insults and is not confined by the extreme polemics of either apoptosis or necrosis.

### 4.2. Therapeutic utility of mitochondriotoxic CPP

MitP penetrates plasma membranes to bind intracellular targets that promote cellular apoptosis. Such mitochondriotoxic properties provide advancements in the design of novel and potent cell penetrant inducers of apoptosis. One of the major drawbacks to the clinical relevance of CPPs has lain in their susceptibility to proteolysis. However, various strategies have been successfully employed, to combat premature degradation, such as incorporation of D-amino acids and retroinverso transformation [37]. So, since the first serendipitous discovery of CPPs some 20 years ago, we are beginning to embrace an era of CPPs in drug development. For instance, cell penetrant

Fig. 5. Z-Gly-RGD*f*-mitP: Cytotoxicity profiles and intracellular translocation. (A) Z-Gly-RGD*f*-mitP demonstrates an enhanced cytotoxic potency compared to mitP and the sequence variant Z-Gly-RGE*f*-mitP. ECV304 cells were exposed to increasing concentrations of peptides (0.1–30 μM) for 24 h. Cell viability was measured by MTT conversion and expressed as a percentage of those cells treated with vehicle (medium) alone. Data points are mean±S.E.M. from 3 experiments performed in triplicate. (B) Specificity of Z-Gly-RGD*f*-mitP for integrins as confirmed by antagonism with cyclo(-RGD*f*V). ECV304 cells were pre-incubated with 300 nM cyclo (-RGD*f*V) for 20 min prior to the addition of increasing concentrations of Z-Gly-RGD*f*-mitP for a further 2 h. Data are expressed as above. (C) Z-Gly-RGD*f*-mitP enhances the potency of mitP in U373MG. Cells were treated with peptides for 24 h and data are expressed as above. (D) Z-Gly-RGD*f*-mitP induces apoptosis of ECV304 and U373MG as confirmed by in situ TUNEL assay. Cells were exposed to 10 μM peptide for 2 h and treated as in Fig. 2A. Control data are also shown in Fig. 2A. Bars are 20 μm. (E) Fluo-Gly-RGD*f*-mitP translocates plasma membranes of ECV304 (bar 5 μm) and U373MG (bar 10 μm) cells. Live confocal cell imaging was captured 45 min after the addition of 5 μM fluorescein-labelled peptide, shown here in green. Cellular distributions of Fluo-Gly-RGD*f*-mitP are presented here merged with images taken under transmission differential interference contrast microscopy.

constructs for the treatment of cardiac ischaemia are now entering clinical trials [38], an advancement that is of no doubt testament to their clinical applicability.

Delivered as message address constructs, our apoptotic chimeric mitP analogues demonstrated enhanced potencies compared to the parent cytotoxin alone and are thus of potential
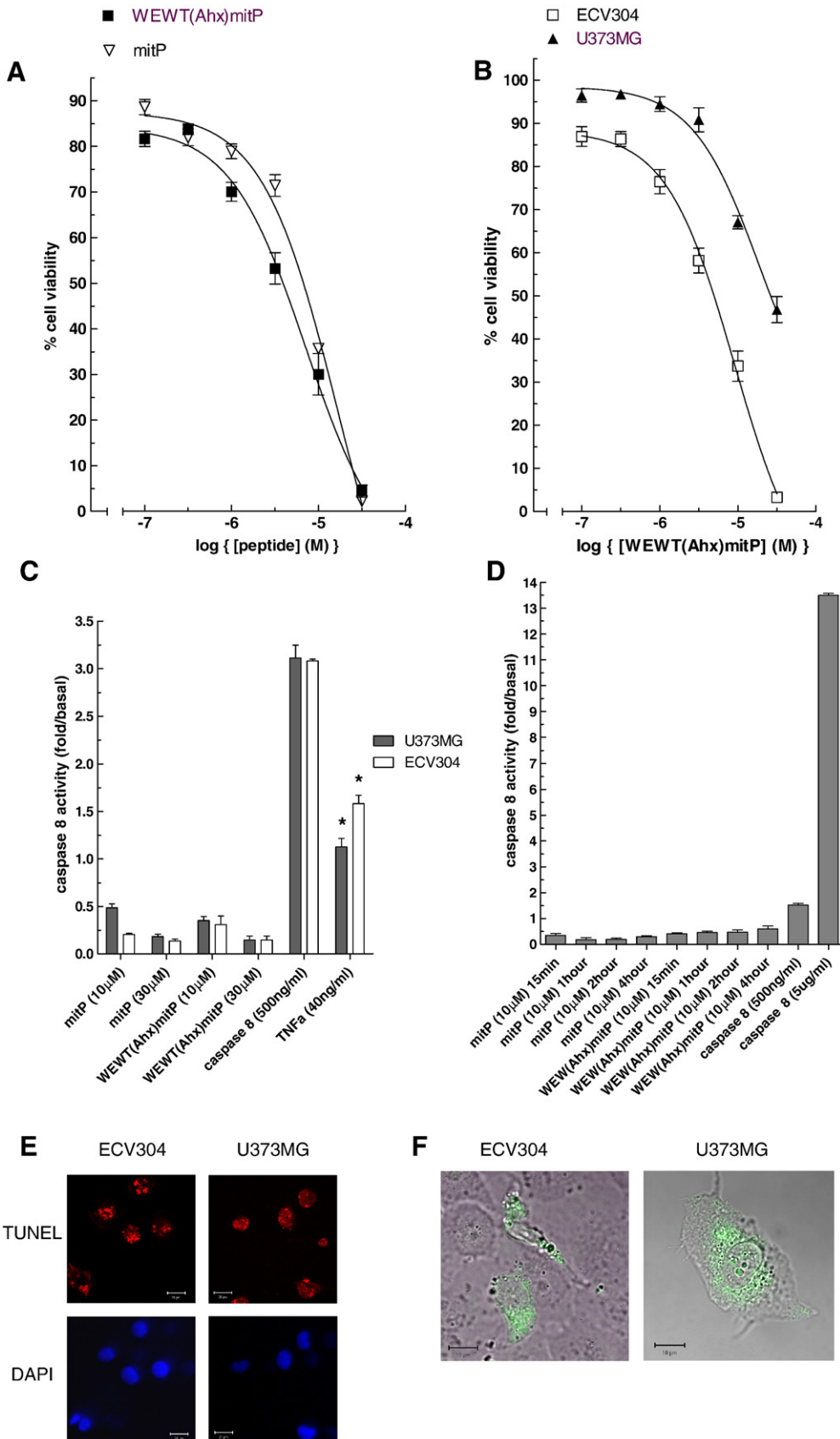
clinical relevance. Moreover, and as stated above, by their very nature, peptides are hydrolyzed readily by endopeptidases. However, this apparent drawback would appear to be advantageous in the case of aggressive malignancies were in situ anti-tumour drug delivery is currently being practiced, demonstrating low toxicity to nearby tissues and avoidance of multiple drug resistance. In addition, tumour specific targeting by peptidyl address motifs could enhance the selectivity of drug delivery leading to a probable reduction in non-selective side-effects.

Previous reports show MP, as part of a tumour targeting liposomal complex, to be effective at concentrations of 25 μM [15]. In comparison, we demonstrate an enhanced potency of mitP on ECV304 and U373MG, with LD_{50}s of 6.81 μM and 7.92 μM respectively and more dramatically so as a sychnologic construct with the RGD address motif, giving LD_{50}s of 1.40 μM and 4.79 μM. Moreover, the enhanced potency demonstrated by Z-Gly-RGDf-mitP on ECV304 of 1.40 μM is easily achievable in vivo. Thus, we have a highly potent mitochondriotoxic CPP and a structure that easily incorporates into a tissue specific construct without impacting upon the bioactivity of the cytotoxin.

Recent findings have indicated that some CPPs are excluded from mitochondrial matrices [39]. Nevertheless, such studies have restricted their observations to limited numbers of CPPs such as the polycationic sequences derived from the HIV-1 transactivator protein, Tat(48–60) and the homeodomain of the homeoprotein Antennapaedia, penetratin (43–58). Furthermore, it is now apparent that there is no uniform mechanism of CPP uptake. Diverse mechanisms include both endocytotic and non-endocytotic mechanisms, energy dependent and translocation occurring at 4 °C and in the absence of ATP. Also, chimeric CPP, consisting of CPP and cargo can adopt quite different mechanisms of uptake to that of the parent CPP [40].

The degree of endosomal sequestration appears to be problematic when delivering CPP or CPP-conjugated cargo and is a matter still open to debate. However, studies that clearly show a robust biological response, as is the case with our mitochondriotoxic CPP, also demonstrate avoidance of endosomal entrapment. In addition, conclusions reached showing that CPPs are not internalized into mitochondria were based not only on live cell imaging colocalization studies but also on isolated mitochondria [39]. However data presented here, for mitP, clearly show mitochondrial targeting and internalization in both isolated systems and live cell imaging, respectively.

4.3. Differential pharmacodynamic parameters of chimeric mitoparan analogues

Pre-incubation of ECV304 cells with the integrin antagonist cyclo(-RGDfV) reduced the cytotoxic potency of Z-Gly-RGDf-mitP and indicated specificity of the chimeric peptide Z-Gly-RGDf-mitP for integrin receptors expressed on ECV304. Similarly, the reduced potency shown by the sequence variant Z-Gly-RGEf-mitP, further suggests integrin-mediated binding for the Z-Gly-RGDf-mitP peptide.

Z-Gly-RGDf-mitP proved to be the most potent of all analogues tested. The ability of this chimera to specifically target integrins, leading to an increased propensity for plasma membrane insertion, may account for this observation. Alternatively, Z-Gly-RGDf-mitP was rationally designed to maintain the amphipathicity of mitP. Moreover, the additional cationic charge provided by Arg[2] of the RGD motif would increase amphipathicity, thus leading to enhanced cellular penetration. Furthermore, N-terminal blockade with Z-Gly, an amidated C-terminal and incorporation of DPhe, will improve the biostability of this chimera. Thus, protease resistance may also contribute to the enhanced bioactivity of this chimeric analogue.

The enhanced potency of WEWT(Ahx)mitP with ECV304 cells compared to U373MG was considered to be a consequence of U373MG being resistant to Fas-mediated apoptosis [34]. An observation that led to the assumption that this mitP analogue was mediating apoptotic events in ECV304 cells, in part, through the extrinsic cell death pathway. However, WEWT(Ahx)mitP did not activate caspase-8 in ECV304 cells. Likewise, WEWT(Ahx)mitP did not activate caspase-8 in U373MG cells. It is significant that U373MG cells are mutant p53 glioma cells. Not only is Fas-mediated apoptosis compromised at the level of caspase-8 [34], but in p53 deficient cell lines, Fas expression is diminished both at the level of transcription and the fully translated cell membrane protein [35]. A decreased cell surface expression of Fas in U373MG cells may account for the reduced potency observed for WEWT(Ahx)mitP ($LD_{50}=28.10$ μM) compared to mitP ($LD_{50}=7.92$ μM) on U373MG cells and WEWT(Ahx)mitP on ECV304 cells ($LD_{50}=6.81$ μM). This observation confirms cell surface markers/binding sites as a pre-requisite for the bioactivity of our addressed apoptotic chimeric analogues. Not only is the potency of WEWT(Ahx)mitP reduced in cells where Fas is compromised but, as is the case with WEWT(Ahx)mitP, the potency of the parent cytotoxin (mitP) is lessened. This latter feature is advantageous when cell-specific delivery is required.

Fig. 6. WEWT(Ahx)mitP: Cytotoxicity profiles and intracellular translocation. (A) N-terminal extension of mitP with WEWT via an Ahx linker moderately enhances the cytotoxic potency of mitP in ECV304 cells. (B) The Fas-mediated apoptotic resistant cell line U373MG demonstrates a decreased potency to WEWT(Ahx)mitP compared to ECV304. Both cell lines were exposed to increasing concentrations of peptides (0.1–30 μM) for 24 h. Cell viability was measured by MTT conversion and expressed as a percentage of those cells treated with vehicle (medium) alone. Data points are mean±S.E.M. from 3 experiments performed in triplicate. (C) WEWT(Ahx)mitP (10 μM, 30 μM) does not activate caspase-8 in ECV304 or U373MG cells, whilst both cell lines are resistant to activation of caspase-8 by the parent cytotoxin mitP. Cells were treated with peptide for 30 min and assayed for caspase-8 activity using the Caspase-8 Colorimetric Assay (R & D Systems). A recombinant caspase-8 enzyme (R & D Systems) was used as a positive control and TNF-α (exposure time of 24 h) as a receptor-mediated activator of caspase-8. Asterisks indicate significantly different means, $P=0.0159$. (D) Temporal analysis up to 4 h, shows that treatment of ECV304 cells with WEWT(Ahx)mitP (10 μM) and mitP (10 μM) does not activate caspase-8. (E) WEWT(Ahx)mitP induces apoptosis of ECV304 and U373MG as confirmed by in situ TUNEL assay. Cells were exposed to 10 μM peptide for 2 h and treated as in Fig. 2A. Control data are also shown in Fig. 2A. Bars are 20 μm. (F) Fluo-WEWT(Ahx)mitP translocates plasma membranes of ECV304 and U373MG cells. Live confocal cell imaging was captured 45 min after the addition of 5 μM fluorescein-labelled peptide, shown here in green. Cellular distributions of Fluo-WEWT(Ahx)mitP are presented here merged with images taken under transmission differential interference contrast microscopy. Bars are 10 μm.

We conclude that the mitochondriotoxic properties of mitP, and the improved pharmacodynamic parameters of chimeric mitP analogues, offer utility for the study and therapeutic induction of apoptosis in human cancer cells.

Acknowledgements

References

[1] T. Higashijima, K. Wakamatsu, M. Takemitsu, M. Fujino, T. Nakajima, T. Miyazawa, Conformational change of mastoparan from wasp venom on binding with phospholipid membrane, FEBS Lett. 152 (1983) 227–230.

[2] Y. Hori, M. Demura, M. Iwadate, A.S. Ulrich, T. Niidome, H. Aoyagi, T. Asakura, Interaction of mastoparan with membranes studied by 1H-NMR spectroscopy in detergent micelles and by solid-state 2H-NMR and 15N-NMR spectroscopy in oriented lipid bilayers, Eur. J. Biochem. 268 (2001) 302–309.

[3] B.C. Suh, S.K. Song, Y.K. Kim, K.T. Kim, Induction of cytosolic Ca^{2+} elevation mediated by Mas-7 occurs through membrane pore formation, J. Biol. Chem. 271 (1996) 32753–32759.

[4] R.M. Epand, Y. Shai, J.P. Segrest, G.M. Anantharamaiah, Mechanisms for the modulation of membrane bilayer properties by amphipathic helical peptides, Biopolymers 37 (1995) 319–338.

[5] K. Nicolay, L.F. Laterveer, W.L. van Heerde, Effects of amphipathic peptides, including presequences, on the functional integrity of rat liver mitochondrial membranes, J. Bioenerg. Biomembr. 26 (1994) 327–334.

[6] D.R. Pfeiffer, T.I. Gudz, S.A. Novgorodov, W.L. Erdahl, The peptide mastoparan is a potent facilitator of the mitochondrial permeability transition, J. Biol. Chem. 270 (1995) 4923–4932.

[7] L. He, J.J. Lemasters, Heat shock suppresses the permeability transition in rat liver mitochondria, J. Biol. Chem. 278 (2003) 16755–16760.

[8] H.M. Ellerby, S.J. Martin, L.M. Ellerby, S.S. Naiem, S. Rabizadeh, G.S. Salvesen, C.A. Casiano, N.R. Cashman, D.R. Green, D.E. Bredesen, Establishment of a cell-free system of neuronal apoptosis: comparison of premitochondrial, mitochondrial, and postmitochondrial phases, J. Neurosci. 17 (1997) 6165–6178.

[9] B.S. Chapman, A region of the 75 kDa neurotrophin receptor homologous to the death domains of TNFR-I and Fas, FEBS Lett. 374 (1995) 216–220.

[10] T. Higashijima, J. Burnier, E. Ross, Regulation of Gi and Go by mastoparan, related amphiphilic peptides, and hydrophobic amines, Mechanism and structural determinants of activity, J. Biol. Chem. 265 (1990) 14176–14186.

[11] K. Wakamatsu, A. Okada, T. Miyazawa, M. Ohya, T. Higashijima, Membrane-bound conformation of mastoparan-X, a G-protein-activating peptide, Biochemistry 31 (1992) 5654–5660.

[12] G.M. Yan, S.Z. Lin, R.P. Irwin, S.M. Paul, Activation of G proteins bidirectionally affects apoptosis of cultured cerebellar granule neurons, J. Neurochem. 65 (1995) 2425–2431.

[13] S. Jones, J. Howl, Biological applications of the receptor mimetic peptide mastoparan, Curr. Protein Pept. Sci. 7 (2006) 501–508.

[14] M. Pooga, M. Hällbrink, M. Zorko, U. Langel, Cell penetration by transportan, FASEB J. 12 (1998) 67–77.

[15] Y. Yamada, Y. Shinohara, T. Kakudo, S. Chaki, S. Futaki, H. Kamiya, H. Harashima, Mitochondrial delivery of mastoparan with transferrin liposomes equipped with a pH-sensitive fusogenic peptide for selective cancer therapy, Int. J. Pharm. 303 (2005) 1–7.

[16] S. Jones, J. Howl, Charge delocalisation and the design of novel mastoparan analogues: enhanced cytotoxicity and secretory efficacy of [Lys[5], Lys[8], Aib[10]]MP, Regul. Pept. 121 (2004) 121–128.

[17] H. Ellerby, W. Arap, L.M. Ellerby, R. Kain, R. Andrusiak, G.D. Rio, S. Krajewski, C.R. Lombardo, R. Rao, E. Ruoslahti, D.E. Bredesen, R. Pasqualini, Anti-cancer activity of targeted pro-apoptotic peptides, Nat. Med. 5 (1999) 1032–1038.

[18] P. Laakkonen, M.E. Akerman, H. Biliran, M. Yang, F. Ferrer, T. Karpanen, R.M. Hoffman, E. Ruoslahti, Antitumor activity of a homing peptide that targets tumor lymphatics and tumor cells, Proc. Natl. Acad. Sci. U. S. A. 101 (2004) 9381–9386.

[19] E. Ruoslahti, M. Pierschbacher, New perspectives in cell adhesion: RGD and integrins, Science 238 (1987) 491–497.

[20] T.I. Samoylova, V.A. Petrenko, N.E. Morrison, L.P. Globa, H.J. Baker, N.R. Cox, Phage probes for malignant glial cells, Mol. Cancer Ther. 2 (2003) 1129–1137.

[21] E. Genersch, M. Ferletta, I. Virtanen, H. Haller, P. Ekblom, Integrin avb3 binding to human a5-laminins facilitates FGF-2- and VEGF-induced proliferation of human ECV304 carcinoma cells, Eur. J. Cell Biol. 82 (2003) 105–117.

[22] S. Tanuma, A. Yoshimori, R. Takasawa, Genomic drug discovery for apoptosis regulation using a new computer screening amino acid complement wave method, Biol. Pharm. Bull. 27 (2004) 968–973.

[23] A. Yoshimori, R. Takasawar, A. Hayakawa, M. Mizuno, J. Yoshida, S. Tanuma, Structure-based design of an agonistic peptide targeting Fas, Apoptosis 10 (2005) 323–329.

[24] R. Schwyzer, ACTH: a short introductory review, Ann. N. Y. Acad. Sci. 297 (1977) 3–26.

[25] J. Howl, M. Wheatley, V1a vasopressin receptors: selective biotinylated probes, Methods Neurosci. 13 (1993) 281–296.

[26] J. Carmichael, W.G. DeGraff, A.F. Gazdar, J.D. Minna, J.B. Mitchell, Evaluation of a tetrazolium-based semiautomated colorimetric assay: assessment of chemosensitivity testing, Cancer Res. 47 (1987) 936–942.

[27] A.S. Belzacq, H.L. Vieira, F. Verrier, G. Vandecasteele, I. Cohen, M.C. Prévost, E. Larquet, F. Pariselli, P.X. Petit, A. Kahn, R. Rizzuto, C. Brenner, G. Kroemer, Bcl-2 and Bax modulate adenine nucleotide translocase activity, Cancer Res. 63 (2003) 541–546.

[28] A. Tarze, A. Deniaud, M. Le Bras, E. Maillier, D. Molle, N. Larochette, N. Zamzami, G. Jan, G. Kroemer, C. Brenner, GAPDH, a novel regulator of the pro-apoptotic mitochondrial membrane permeabilization, Oncogene 26 (2007) 2606–2620.

[29] A. Deniaud, C. Rossi, A. Berquand, J. Homand, S. Campagna, W. Knoll, C. Brenner, J. Chopineau, Voltage-dependent anion channel transports calcium ions through biomimetic membranes, Langmuir 23 (2007) 3898–3905.

[30] F.P. Thinnes, H. Florke, H. Winkelbach, U. Stadtmüller, M. Heiden, A. Karabinos, D. Hesse, H.D. Kratzin, E. Fleer, N. Hilschmann, Channel active mammalian porin, purified from crude membrane fractions of human B lymphocytes or bovine skeletal muscle, reversibly binds the stilbene-disulfonate group of the chloride channel blocker DIDS, Biol. Chem. Hoppe-Seyler 375 (1994) 315–322.

[31] A.P. Halestrap, C.P. Connern, E.J. Griffiths, P.M. Kerr, Cyclosporin A binding to mitochondrial cyclophilin inhibits the permeability transition pore and protects hearts from ischaemia/reperfusion injury, Mol. Cell. Biochem. 174 (1997) 167–172.

[32] C.F. Yang, H.M. Shen, C.N. Ong, Intracellular thiol depletion causes mitochondrial permeability transition in ebselen-induced apoptosis, Arch. Biochem. Biophys. 380 (2000) 319–330.

[33] M. Gurrath, G. Muller, H. Kessler, M. Aumailley, R. Timpl, Conformation/activity studies of rationally designed potent anti-adhesive RGD peptides, Eur. J. Biochem. 210 (1992) 911–912.

[34] M.J. Knight, C.D. Riffkin, A.M. Muscat, D.M. Ashley, C.J. Hawkins, Analysis of FasL and TRAIL induced apoptosis pathways in glioma cells, Oncogene 20 (2001) 5789–5798.

[35] J.A. Cerrato, T. Khan, D. Koul, F.F. Lang, C.A. Conrad, W.K. Yung, T.J. Liu, Differential activation of the Fas/CD95 pathway by Ad-p53 in human gliomas, Int. J. Oncol. 24 (2004) 409–417.

[36] J.J. Lemasters, V. Necrapoptosis and the mitochondrial permeability transition: shared pathways to necrosis and apoptosis, Am. J. Physiol.: Gastrointest. Liver Physiol. 276 (1999) G1–G16.

[37] J. Howl, Z. Prochazka, M. Wheatley, J. Slaninova, Novel strategies for the design of receptor-selective vasopressin analogues: Aib-substitution and retro-inverso transformation, Br. J. Pharmacol. 128 (1999) 647–652.

[38] S. Moschos, A. Williams, M.A. Lindsay, In vivo applications of cell-penetrating peptides, in: U. Langel (Ed.), Handbook of cell penetrating peptides, 2nd Edition, CRC Taylor & Francis, Boca Raton, 2007, pp. 423–438.

[39] M.F. Ross, A. Filipovska, R.A.J. Smith, M.J. Gait, M.P. Murphy, Cell-penetrating peptides do not cross mitochondrial membranes even when conjugated to a lipophilic cation: evidence against direct passage through phospholipid bilayers, Biochem. J. 383 (2004) 457–468.

[40] U. Langel, Handbook of cell-penetrating peptides, 2nd Edition, CRC Taylor & Francis, Boca Raton, 2007.